Journal of Inorganic and General Chemistry
ZAAC
Zeitschrift für anorganische und allgemeine Chemie
www.zaac.wiley-vch.de
RESEARCH ARTICLE

DOI: 10.1002/zaac.202200117

Single Crystal X-Ray Structure Analyses of Binary and Ternary Compounds $A_{49}Tl_{108+x}$ (A = K, Rb, Cs; x = 0–1.76) Related to the $K_{49}Tl_{108}$ Type Structure

Vanessa F. Schwinghammer,[a] Melissa Janesch,[a] Florian Kleemiss,[b] and Stefanie Gärtner*[a, b]

Dedicated to Prof. Dr. Caroline Röhr on the occasion of her 60th birthday.

The structural chemistry of alkali metal thallides shows a broad range of type structures. At an alkali metal : thallium proportion A:Tl 1:2 the perceived dependency on the alkali metal involved is conspicuous. Two main structure types are reported with $A_{15}Tl_{27}$ (A = K, Rb, Cs) and $K_{49}Tl_{108}$. The compound $K_{49}K_{108}$ with a 3-dimensional Tl-substructure has been known since 1993 from Cordier and Müller but so far only with potassium. We here present single crystal X-Ray structure analyses of the compounds $K_{49-y}Rb_yTl_{108}$, and $K_{49-y}Cs_yTl_{108}$ ($y < 10$) belonging to the $K_{49}Tl_{108}$ type structure. Additionally, structures of $Rb_{49}Tl_{109.67}$, $Cs_{3.35}Rb_{45.65}Tl_{109.71}$ and $Cs_{7.49}Rb_{41.51}Tl_{109.76}$ are introduced, which prove the possibility of Tl incorporation in the Tl_{12} icosahedra in $K_{49}Tl_{108}$ type structures. The effects of the change in alkali metals on the thallium substructure are discussed as well as the preferred Wyckoff sites of the different alkali metals.

Introduction

Alkali metal thallides are known since the investigative works of E. Zintl and W. Dullenkopf when they first described the synthesis and characterization of NaTl in 1932.[1,2] Combining an electropositive metal with thallium allows one to gain deeper insights into the structure formation of this heavy main group element.[3] This is especially interesting, as this element is located left to the Zintl border, but the electron counting rules for Zintl phases still are applicable for some of the reported materials. Part of them contains isolated clusters,[4] dependent on the amount of alkali metal involved, also two- and three-dimensional networks are observed.[5] In some compounds, a complete electron transfer from the more electropositive to the electronegative element is assumed to result in a modified valence electron concentration (VEC_{Zintl}) per p-block element.[2,6] The crystal structure can then be described by the (8-N)- rule and the Zintl-Klemm-formalism.[7] This principle works well for the elements right to the Zintl border.[8] But also part of alkali metal thallides follow this model, even thallium is placed left of this imaginary border. In contrast to the elements right to the Zintl border, here a dependency on the alkali metal involved is observed and the calculated valence electron concentration (VEC) does not automatically suggest a thallium substructure. The mixing of trielides provides interesting insights in terms of structural chemistry.[9] The focus of our investigations is set on the different alkali metals, as they do not only serve as counterions for charge balancing reasons but play an essential role in the formation and stabilization of the thallium substructure.[2,10] One discrepancy becomes evident for the ratio of A:Tl 1:2. These materials are known to be metallic and a complete electron transfer from the electropositive to the electronegative element is virtually not true. There are two main type structures described for the ratio A:Tl 1:2. The larger alkali metals rubidium and cesium form $A_{15}Tl_{27}$, which includes thallium substructures explainable by the counting rules after Zintl.[11] Here, Tl_{11}^{7-} clusters and two-dimensional Tl_{16}^{8-} layers are present. We recently could show, that even more thallium can be included in this type structure, which is equivalent to a broader range of possible VEC for $A_{15}Tl_{27}$ type materials. Additionally, it was shown, that potassium can be realized in mixed alkali metal compounds $A_{15}Tl_{27}$ when a larger alkali metal is present. In contrast, the lighter alkali metal potassium forms an intermetallic phase $K_{49}Tl_{108}$ with a three-dimensional thallium substructure, which cannot be explained straightforwardly by the counting rules.[10,12] This makes the discrepancy between $K_{49}Tl_{108}$ and $A_{15}Tl_{27}$ very interesting, as it represents a borderline case between metallic and salt-like compounds. In packing-dominated intermetallic compounds, Frank Kasper polyhedra represent important building blocks.[3] According to this, these polyhedral subunits are also a common feature in many alkali

[a] V. F. Schwinghammer, M. Janesch, Dr. S. Gärtner
Department of Inorganic Chemistry
University of Regensburg
93040 Regensburg (Germany)
E-mail: Stefanie.Gaertner@ur.de
[b] Dr. F. Kleemiss, Dr. S. Gärtner
Central Analytics
University of Regensburg
93040 Regensburg (Germany)

Supporting information for this article is available on the WWW under https://doi.org/10.1002/zaac.202200117

metal thallides, while icosahedra (CN 12) are also typically observed as filled entities M@Tl_{12} (M = Tl,[5,13] Na,[14] Mg, Cd, Hg, Zn[15]). In $K_{49}Tl_{108}$, a three-dimensional thallium substructure is formed by hexagonal antiprisms, which according to Cordier and Müller are interconnected by Tl_4 chains and so form tubes in all three dimensions without intersecting.[16] The generated voids between the tubes are filled with empty Tl_{12} icosahedra.[16]

A related structure was observed for the lighter homologue indium in the compound $A_3Na_{26}In_{48}$ (A = K, Rb, Cs).[17] Hexagonal antiprisms form a three-dimensional network and empty In_{12} icosahedra are located in the interstices. In contrast to $K_{49}Tl_{108}$ there are no In_4 chains present.

Results and Discussion

X-Ray Structure Analysis from Single Crystals

We here report on the x-ray structure analysis of seven binary and ternary compounds $Rb_{49}Tl_{109.67}$, $Cs_{2.51}K_{46.49}Tl_{108}$, $Cs_{9.33}K_{39.67}Tl_{108}$, $Rb_{1.57}K_{47.43}Tl_{108}$, $Rb_{8.93}K_{40.07}Tl_{108}$, $Cs_{3.35}Rb_{45.65}Tl_{109.71}$ and $Cs_{7.49}Rb_{41.51}Tl_{109.76}$. Additionally, we prepared literature-known $K_{49}Tl_{108}$ and collected data at 123 K, in order to allow the comparison of obtained distances. All binary and ternary materials crystallize in $K_{49}Tl_{108}$ type related structures (cubic, space group $Pm\bar{3}$). Selected data of the x-ray structure analyses of the characterized crystals are given in Table 1 and Table 2,

Table 1. Selected single crystal data collection and structure refinement parameters for the four compounds $K_{47.43}Rb_{1.57}Tl_{108}$, $K_{40.07}Rb_{8.93}Tl_{108}$, $K_{46.49}Cs_{2.51}Tl_{108}$ and $K_{39.67}Cs_{9.33}Tl_{108}$.

Empirical formula	$K_{47.43}Rb_{1.57}Tl_{108}$	$K_{40.07}Rb_{8.93}Tl_{108}$	$K_{46.49}Cs_{2.51}Tl_{108}$	$K_{39.67}Cs_{9.33}Tl_{108}$
CSD number	2157454	2157533	2157504	2157731
Formula weight	24061.12	24403.99	24225.37	24863.11
Temperature/K	123	123	123	123
Crystal system	cubic	cubic	cubic	cubic
Space group	$Pm\bar{3}$	$Pm\bar{3}$	$Pm\bar{3}$	$Pm\bar{3}$
a/Å	17.1677(2)	17.19580(10)	17.2337(2)	17.2846(2)
Volume/Å^3	5059.83(18)	5084.72(9)	5118.42(18)	5163.90(18)
Z	1	1	1	1
ρ_{calc}/(g/cm^3)	7.9	8.0	7.9	8.0
Radiation λ/Å	AgKα 0.56087	AgKα 0.56087	AgKα 0.56087	MoKα 0.71073
μ/mm^{-1}	47.0	47.6	46.5	86.3
Independent reflections	4417	8341	4483	2107
Goodness-of-fit on F^2	1.103	1.111	1.084	1.214
R_{int}	0.0602	0.0435	0.0501	0.0674
Final R indexes [I >= 2σ (I)]	R_1 = 0.0224, wR_2 = 0.0462	R_1 = 0.0266, wR_2 = 0.0569	R_1 = 0.0240, wR_2 = 0.0494	R_1 = 0.0450, wR_2 = 0.0652
Final R indexes [all data]	R_1 = 0.0282, wR_2 = 0.0478	R_1 = 0.0366, wR_2 = 0.0598	R_1 = 0.0336, wR_2 = 0.0524	R_1 = 0.0633, wR_2 = 0.0703
Largest diff. peak/hole/e Å^{-3}	3.41/−1.79	7.70/−4.87	2.73/−3.53	7.96/−2.42

Table 2. Selected single crystal data collection and structure refinement parameters for the four compounds $K_{49}Tl_{108}$, $Rb_{49}Tl_{109.67}$, $Cs_{3.35}Rb_{45.65}Tl_{109.71}$ and $Cs_{7.49}Rb_{41.51}Tl_{109.76}$.

Empirical formula	$K_{49}Tl_{108}$	$Rb_{49}Tl_{109.67}$	$Cs_{3.35}Rb_{45.65}Tl_{109.71}$	$Cs_{7.49}Rb_{41.51}Tl_{109.76}$
CSD number	2157706	2157529	2157732	2157743
Formula weight	23989.90	26668.73	26768.38	26975.01
Temperature/K	123	123	123	123
Crystal system	cubic	cubic	cubic	cubic
Space group	$Pm\bar{3}$	$Pm\bar{3}$	$Pm\bar{3}$	$Pm\bar{3}$
a/Å	17.17550(10)	17.5761(3)	17.6125(3)	17.6360(5)
Volume/Å^3	5066.73(9)	5429.6(3)	5463.4(3)	5485.3(5)
Z	1	1	1	1
ρ_{calc}/(g/cm^3)	7.9	8.2	8.1	8.2
Radiation λ/Å	MoKα 0.71073	AgKα 0.56087	AgKα 0.56087	AgKα 0.56087
μ/mm^{-1}	86.5	49.8	49.3	50.0
Goodness-of-fit on F^2	1.114	1.132	1.166	0.984
Unique reflections	3756	4749	4768	3238
R_{int}	0.0547	0.0417	0.0681	0.0622
Final R indexes [all data]	R_1 = 0.0395, wR_2 = 0.0847	R_1 = 0.0223 wR_2 = 0.0380	R_1 = 0.0461, wR_2 = 0.0492	R_1 = 0.0279, wR_2 = 0.0331
Final R indexes [I >= 2σ (I)]	R_1 = 0.0538, wR_2 = 0.0894	R_1 = 0.0316 wR_2 = 0.0402	R_1 = 0.0650, wR_2 = 0.0520	R_1 = 0.0461, wR_2 = 0.0356
Largest diff. peak/hole/e Å^{-3}	5.13/−7.68	2.54/−1.75	2.14/−3.26	2.35/−2.15

for more detailed information see supporting information. These compounds naturally feature large absorption coefficients for x-rays, therefore small single crystals were selected and Ag Kα radiation was used depending on availability. The still remaining absorption effects could be reduced by carefully applying absorption correction by the diffractometer software (*CrysAlisPro*).[18]

During our research on the mixed $A_{15}Tl_{27}$ phases, we observed the first ternary compounds in the $K_{49}Tl_{108}$ type structure as a byproduct.[10] With an alkali metal proportion of approximately 33 % (*A*:Tl∼1:2) its valence electron concentration is very similar to the one from $A_{15}Tl_{27}$ (VEC∼2.33) and therefore both phases are observed in the powder diffraction pattern (see SI).

In $K_{49}Tl_{108}$ two main entities concerning the thallium substructure are present. The three-dimensional thallium network is built by hexagonal antiprisms, which together with a Tl_4 chain build interconnected tubes in all spatial directions (see Figure 1). In the generated interstices two Tl_{12} icosahedra can be found, which are generated by one symmetry inequivalent Tl position (Wyckoff positions 12*j* and 12*k*). These icosahedra are located at the corners and in the center of the unit cell. The alkali metals reside in six different Wyckoff positions. In the following, the thallium substructure, as well as the involved alkali metals are discussed more in detail. In general, the cell volume increases with the proportion of potassium substituted by larger alkali metals, taking into account the different sizes of Rb and Cs, respectively.

Occupation Trends of the Alkali Metal Positions

In the type structure $K_{49}Tl_{108}$ there exist six symmetry-inequivalent alkali metal positions. These have different environments, resulting in different occupation tendencies when mixing the alkali metals. Having a closer look at the near surroundings of the six alkali metal positions reveals, that the coordination sphere varies from 15 to 16 to 20 neighboring atoms (Figure 2). While the coordination numbers of 15 and 16 are according to the number found in Frank-Kasper polyhedra,[19] the number of 20 for alkali metal position *A*6 is conspicuous.

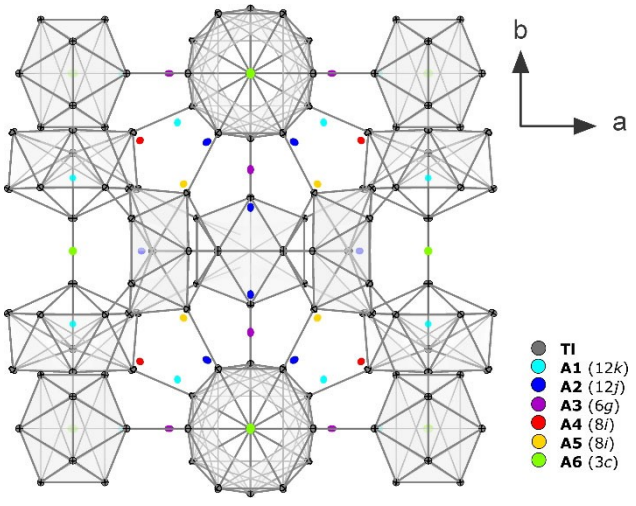

Figure 1. Unit cell of the $K_{49}Tl_{108}$ type structure with the six symmetry-inequivalent alkali metal positions.

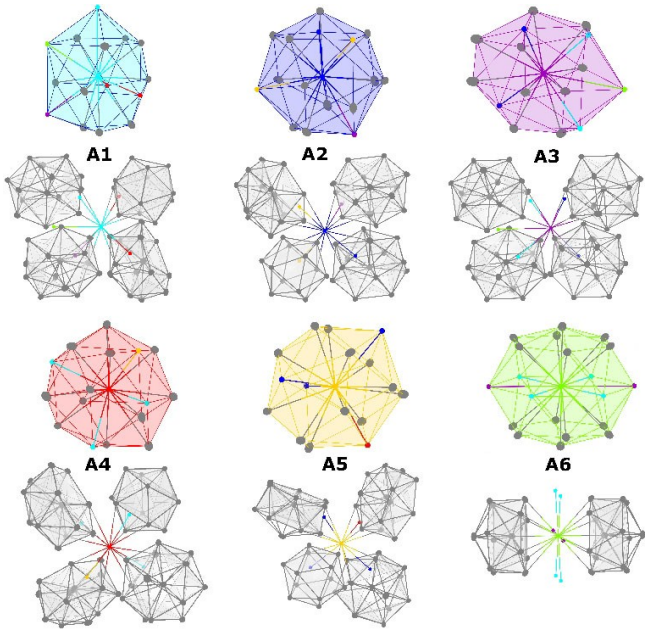

Figure 2. Surroundings of the six symmetry-inequivalent alkali metal positions in $A_{49}Tl_{108}$.

While alkali metal positions *A*1 to *A*5 coordinate to four different Tl substructural building blocks (hexagonal antiprism or icosahedra), *A*6 on Wyckoff position 3*c* is located between two centered hexagonal antiprisms and as a consequence a number of 14 coordinating Tl atoms are present. The coordination sphere is completed by six alkali metals (*A*2 and *A*3). The distances to the 20 neighboring atoms are longer compared to the remaining alkali metals and as a consequence, this results in more space for alkali metals residing at the *A*6 position.[2] The compounds $Cs_{2.51}K_{46.49}Tl_{108}$ and $Rb_{1.57}K_{47.43}Tl_{108}$ confirm that *A*6 is preferably substituted by heavier alkali metals. In general, the occupational trend of the position of the larger alkali metal follows the sequence *A*6 > *A*5 > *A*4 > *A*2 > *A*3 > *A*1 (Table 3). In the compounds $K_{40.07}Rb_{8.93}Tl_{108}$ and $Cs_{3.35}Rb_{45.65}Tl_{109.71}$ on alkali metal position *A*1 (and *A*2 and *A*3) no mixed occupation K/Rb or Cs/Rb is described. Mixed occupancy cannot be ruled out, as the s.o.f. (=site occupancy factor) of rubidium was not significant when applying split positions.

Discussion of the Tl_4-Chain

Cordier and Müller described the structure of $K_{49}Tl_{108}$ containing tubes generated by hexagonal antiprisms, which are connected by Tl_4 chains (Tl8–Tl7–Tl7–Tl8) to form dumbbells (see Figure 3).[16] This is justified by the very similar d(Tl7–Tl7) and d(Tl7–Tl8) distances. In our series we obtained increasing

Table 3. Site occupancy factors (s.o.f.) of the symmetry-inequivalent alkali metal positions of the mixed alkali metal thallides of the $K_{49}Tl_{108}$ type structure.

Compound	A1 (12k)	A2 (12k)	A3 (6 g)	A4 (8i)	A5 (8i)	A6 (3d)
$K_{49}Tl_{108}$	K 1	K 1	K 1	K 1	K 1	K 1
$Rb_{1.57}K_{47.43}Tl_{108}$	K 1	K 1	K 1	K 1	K 1	K 0.475(14) Rb 0.525(14)
$Rb_{8.93}K_{40.07}Tl_{108}$	K 1	K 0.809(5) Rb 0.191(5)	K 0.912(8) Rb 0.088(8)	K 0.808(6) Rb 0.192(6)	K 0.752(7) Rb 0.248(7)	K 0.135(12) Rb 0.865(12)
$Cs_{2.51}K_{46.49}Tl_{108}$	K 1	K 1	K 1	K 1	K 1	K 0.162(8) Cs 0.838(8)
$Cs_{9.33}K_{39.67}Tl_{108}$	K 1	K 0.815(11) Cs 0.185(11)	K 1	K 0.790(13) Cs 0.210(13)	K 0.696(13) Cs 0.304(13)	Cs 1
$Rb_{49}Tl_{109.67}$	Rb 1	Rb 1	Rb 1	Rb 1	Rb 1	Rb 1
$Cs_{3.35}Rb_{45.65}Tl_{109.71}$	Rb 1	Rb 1	Rb 1	Rb 0.892(11) Cs 0.108(11)	Rb 0.844(11) Cs 0.155(11)	Rb 0.586(19) Cs 0.414(19)
$Cs_{7.49}Rb_{41.51}Tl_{109.76}$	Rb 1	Rb 0.849(9) Cs 0.151(9)	Rb 1	Rb 0.762(11) Cs 0.238(11)	Rb 0.723(11) Cs 0.277(11)	Rb 0.478(19) Cs 0.522(19)

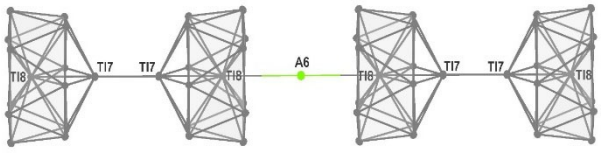

Figure 3. Two pairs of apices-connected, thallium centered mono-capped hexagonal antiprisms. The hexagonal face capping *A*6(3*c*) connects two of these thallium substructures.

Table 4. Selected distances in the hexagonal antiprismatic chain substructure of the eight compounds $K_{49}Tl_{108}$ (1), $K_{47.43}Rb_{1.57}Tl_{108}$ (2), $K_{40.07}Rb_{8.93}Tl_{108}$ (3), $K_{46.49}Cs_{2.51}Tl_{108}$ (4), $K_{39.67}Cs_{9.33}Tl_{108}$ (5), $Rb_{49}Tl_{109.67}$ (6), $Cs_{3.35}Rb_{45.65}Tl_{109.71}$ (7) and $Cs_{7.49}Rb_{41.51}Tl_{109.76}$ (8).

	d(Tl7–Tl7)/Å	d(Tl7–Tl8)/Å	Difference/Å	d(Tl8-*A*6)/Å
1	3.1635(16)	3.1680(12)	0.0045	3.8380(9)
2	3.1691(7)	3.1581(5)	0.011	3.8413(3)
3	3.1740(6)	3.1549(4)	0.0191	3.8560(3)
4	3.1612(8)	3.1482(6)	0.013	3.8881(3)
5	3.181(3)	3.151(2)	0.03	3.9003(14)
6	3.2281(7)	3.1871(5)	0.041	3.9851(4)
7	3.2345(12)	3.1856(8)	0.0489	4.0033(5)
8	3.2391(11)	3.1870(8)	0.0521	4.0115(5)

differences for these distances when larger alkali metals were present (Table 4). In mixed K/Rb or K/Cs compounds with cesium or rubidium on *A*6, the Tl7–Tl8 distance is slightly smaller compared to the binary $K_{49}Tl_{108}$, whereas the Tl7–Tl7 distance correlates directly with the dimensions of the unit cell edge. Therefore, we would prefer to describe this structural entity as thallium centered, mono-capped hexagonal antiprisms rather than a Tl_4 chain, as this consideration would allow the changes according to the unit cell edge.

Centre Occupation of the Tl3/Tl4 Icosahedra

The two crystallographically different icosahedral subunits in $A_{49}Tl_{108}$ are each built via one symmetry-inequivalent Tl site (Tl3 and Tl4) due to the high symmetry of space group $Pm\bar{3}$. While in $K_{49}Tl_{108}$ empty icosahedra are present, we observed some low residual electron density in the center of the Tl3 icosahedra for the ternary compound $K_{47.43}Rb_{1.57}Tl_{108}$. Subsequent analyses of the remaining ternaries including potassium showed similar features. Altogether, in all ternary compounds including potassium ($Cs_{2.51}K_{46.49}Tl_{108}$, $Cs_{9.33}K_{39.67}Tl_{108}$, $Rb_{1.57}K_{47.43}Tl_{108}$, $Rb_{8.93}K_{40.07}Tl_{108}$), residual electron density could be observed in at least one of the centers of the two different icosahedra. This led to the idea of additional thallium atoms might be realizable in $A_{49}Tl_{108}$ type materials, which occupy the center of the icosahedra ((Tl9, Wyckoff position 1*a*, Tl10 Wyckoff position *1*b). Of course, the very low residual electron density peaks in the potassium including compounds did not prove this and a refinement of thallium at these positions did not yield sites with a significant s.o.f. According to the assumption, that larger icosahedra might allow thallium being present within the icosahedra, we prepared binary approaches with Rb or Cs and a small excess of Tl compared to the *A*:Tl 49:108 stoichiometry . While in the cesium approach only $Cs_{14.53}Tl_{28.4}$ was formed,[10] $Rb_{49}Tl_{109.67}$ was obtained when rubidium was provided, which includes partially filled icosahedral subunits. Centered icosahedra are known as subunits in different binary and ternary thallides and in these cases the central atom is reported as Na,[14] Mg, Cd, Hg, Zn,[15] or Tl.[5,13] The large electron density within the icosahedra in $Rb_{49}Tl_{109.67}$ only can be explained when thallium is incorporated, as the free refinement of rubidium at these positions yields s.o.f. >2. X-Ray absorption effects can be ruled out as different wavelengths have been applied (AgKα, MoKα) which yielded the same s.o.f. for thallium, independent from the wavelength employed. The distance from the central atom to the edges of the icosahedra ($\sim$3.15 Å) would only suggest sodium as alkali metal,[1,20] as according to literature,[2] the remaining alkali metals *A* = K-Cs claim d(*A*–Tl) >3.5 Å. The

presence of additional elements different from rubidium and thallium was excluded by SEM/EDS measurements (see SI). Electronic reasons for the not fully occupied sites within the icosahedra in $Rb_{49}Tl_{109.67}$ cannot be ruled out. In case of smaller Ga, fully occupied thallium icosahedra have been reported recently.[21] Alkali metal mixing of Rb/Cs allowed the characterization of $Cs_{3.35}Rb_{45.65}Tl_{109.71}$ and $Cs_{7.49}Rb_{41.51}Tl_{109.76}$ by single crystal x-ray structure analysis. The observed trend of the unit cell parameters directly correlates with the s.o.f. as well as the distances from the center of the icosahedra to the edges (Table 5).

Single crystal x-ray structure analysis of $Rb_{49}Tl_{109.67}$ allowed the reasonable refinement of the thallium atoms residing in the Tl_{12} cluster units (s.o.f.(Tl9) = 0.792(4), s.o.f.(Tl10) = 0.880(5)). The ternary compound $Cs_{7.49}Rb_{41.51}Tl_{109.76}$ gave the highest thallium content within the icosahedra (s.o.f. of 0.858(6) Tl9 and 0.905(6) Tl10). This trend is also reflected in the dimensions of the respective icosahedron: The larger the alkali metal, the longer the Tl3–Tl3 and Tl4–Tl4 distance and thus the more the icosahedral dimensions increase (Table 5).

The size of the icosahedra of the potassium including compounds ($d(centre-edge) \approx 3.03$ Å) is comparably small. In contrast, the icosahedra of $Rb_{49}Tl_{109.67}$ and both of the mixed Cs/Rb ternaries show significantly larger sizes ($d(Tl(c-e) \approx 3.15$ Å). Apparently, this paves the way for a higher thallium content in the center of the icosahedra.

In order to ensure the refinement of the not fully occupied thallium positions at Wyckoff 1*a* and 1*b*, the residual density was additionally analyzed by inspecting the fractal dimension distribution,[22] which is implemented in NoSpherA2 (Olex2).[23,24]

These plots can be understood as a histogram of isosurface intersections going through the unit cell at a given residual density level. These plots were initially designed for the assessment of charge density models but can be used to assess the overall quality of any crystallographic model. A statistical noise would result in a symmetrically bell-shaped curve around the residual density value of 0, while the wide-ness of the curve tells about the level of noise present in the data. Any one-sided deviation from the bell-shaped curve might hint toward unexplained features of the diffraction data. A strongly negative deformation of the fractal dimension distribution hints toward over-occupied positions, a strong positively sided deviation toward under or misassigned atom positions. Other effects visible in fractal dimensional plots include anharmonicity, scale factor issues or residual bonding density, which are not as relevant in this case. While our model results in a regular bell-shaped curve, the fully occupied sites would give a very irregular fractal dimension distribution plot. The same holds true for the mixed Rb/Cs compounds. This supports our applied

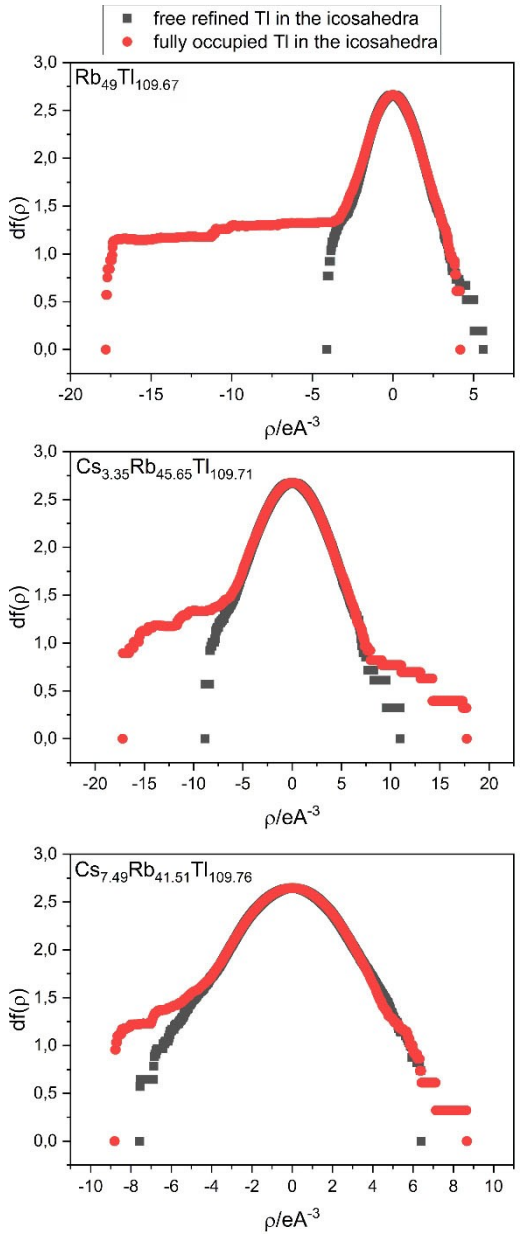

Figure 4. Fractal dimension distributions[22] for $Rb_{49}Tl_{109.67}$, $Cs_{3.35}Rb_{45.65}Tl_{109.71}$ and $Cs_{7.49}Rb4_{1.51}Tl_{109.76}$ support the model for partially filled icosahedra.

Table 5. Selected distances and s.o.f. of the filled icosahedral subunits in $Rb_{49}Tl_{109.67}$ (6), $Cs_{3.35}Rb_{45.65}Tl_{109.71}$ (7) and $Cs_{7.49}Rb_{41.51}Tl_{109.76}$ (8).

	d(Tl3–Tl3)/Å	d(Tl4–Tl4)/Å	d(Tl3–Tl9)/Å	d(Tl4–Tl10)/Å	s.o.f.(Tl9) (1*a*)	s.o.f.(Tl10) (1*b*)
6	3.2634(5) 3.3202(3)	3.1905(5) 3.3400(3)	3.1467(3)	3.1474(2)	0.792(4)	0.880(4)
7	3.2630(8) 3.3227(4)	3.1926(8) 3.3414(4)	3.1485(4)	3.1488(4)	0.823(6)	0.891(6)
8	3.2660(8) 3.3284(4)	3.1965(8) 3.3456(4)	3.1535(4)	3.1528(4)	0.858(6)	0.905(6)

structural model for all three thallides with partially filled icosahedra (Figure 4). In case of the mixed ternary potassium compounds, the free refinement of the electron density in the icosahedral units as thallium atoms did not result in significant values of the s.o.f. The fractal dimension distribution plots might suggest at least for $Cs_{9.33}K_{39.67}Tl_{108}$ an improvement of the model (see SI).

Conclusions

Our investigations on the intermetallic phase $A_{49}Tl_{108+x}$ (A = K, Rb, Cs; x = 0–1.76) gave new insight in the role of the alkali metals in different binary and ternary compounds of mixed alkali metals K/Rb, K/Cs and Rb/Cs in this type structure, which has been known exclusively with potassium. In ternary approaches including potassium, it could be shown that larger alkali metals preferably substitute potassium on the special Wyckoff position 3*g*, which consequently also affects part of the thallium substructure. Additionally, we could demonstrate, that larger alkali metals can be realized in this type structure without potassium being present. In this case, a larger amount of thallium is present. $Rb_{49}Tl_{109.67}$, and $Cs_{4.36}Rb_{44.80}Tl_{109.71}$ and $Cs_{7.49}Rb_{41.51}Tl_{109.76}$ are representatives for potassium-free thallides related to the $K_{49}Tl_{108}$ type structure. The crystal structures of the latter showed that an increasing size of the involved alkali metal causes an enlargement of the unit cell. This allows an incorporation of thallium in the center of both icosahedral substructures of thallium, which are empty in the long known binary compound $K_{49}Tl_{108}$ described by Cordier and Müller in 1993.

Experimental Section

All compounds have been prepared by classical solid-state techniques. The alkali metals cesium and rubidium were obtained by reduction of the alkali metal chlorides with elemental calcium[25] and afterwards distilled twice for purification. Thallium drops (ABCR, purity 99.99%) were used without further purification and were stored under inert gas atmosphere.

Synthesis of the Ternary Compounds: Thallium is known to be very toxic, therefore all manipulations need to minimize the risk of any contamination. Due to the fact that thallides are very sensitive towards air and moisture, all operations are performed under inert gas atmosphere (glove box, inert gas techniques), which reduces the direct contact with this poisonous element. The starting materials were placed in tantalum ampoules and sealed in argon atmosphere. The following stoichiometric proportions have been employed: $Cs_3K_{12}Tl_{27}$, $CsK_{14}Tl_{27}$, $RbK_{14}Tl_{27}$, $Rb_3K_{12}Tl_{27}$, $Cs_2Rb_{13}Tl_{27}$ and $Cs_3Rb_{12}Tl_{27}$. The sealed ampoules then were placed in quartz glass tubes (QSIL GmbH, Ilmenau, Germany) and sealed again under argon atmosphere. For all ternary compounds the same temperature program was used: heating up from room temperature to 973.15 K with a heating rate of 100 K/h, holding for 24 h and cooling to room temperature with a rate of 3 K/h. Due to their high sensitivity toward moisture and oxygen, they were stored in a glove box. (Labmaster 130 G Fa. M. Braun, Garching, Germany).

Synthesis of $Rb_{49}Tl_{109.67}$: The synthesis of the binary compound $Rb_{49}Tl_{109.67}$ was carried out at a different temperature program: heating up from room temperature to 723.15 K with a heating rate of 50 K/h, holding for 24 h and cooling to room temperature with a rate of 25 K/h. Due to their high sensitivity towards moisture and oxygen, they were stored in a glove box. (Labmaster 130 G Fa. M. Braun, Garching, Germany). Different stoichiometric proportions according to $Rb_{49}Tl_{110}$, $Rb_{49}Tl_{112}$ and $Rb_{49}Tl_{115}$ all yielded $Rb_{49}Tl_{109.67}$ beside different amounts of $Rb_{15}Tl_{27}$.

X-ray Diffraction Studies: To characterize the products using single crystal X-ray diffraction, a small number of crystals were transferred into dried mineral oil. Thereafter, a suitable crystal was selected and mounted on a Rigaku SuperNova diffractometer (Rigaku Polska Sp. Z o. o. UI, Wroclaw, Poland) (X-ray: Mo & Ag microfocus, Eos detector in case of Mo, AtlasS2 in case of Ag) using MiTeGen loops. All data were collected at 123 K.

The software *CrysAlisPro* (Version 41_64.93a) was used for data collection and data reduction.[18] For structure solution *ShelXT*[26] was used and the subsequent data refinement was carried out with *ShelXL*.[27] Olex2[24] was taken for visualization purposes and the software Diamond4[28] was chosen for representation of the crystal structure. All atoms are depicted as ellipsoids with a 50% probability level.

Crystallographic data for the compounds have been deposited in the Cambridge Crystallographic Data Center, CCDC, 12 Union Road, Cambridge CB21EZ, UK. Copies of the data can be obtained free of charge under the depository number CCDC-2103387 (Fax: +44-1223-336-033, E-Mail: deposit@ccdc.cam.ac.uk, http://www.ccdc.cam.ac.uk).

Powder Diffraction Studies: Powder diffraction samples were prepared in sealed capillaries (Ø 0.3 mm, WJM-Glas-Müller GmbH, Berlin, Germany). The data collection was carried out on a STOE Stadi P diffractometer (STOE, Darmstadt, Germany) (monochromatic MoKα1 radiation, λ = 0.70926 Å) equipped with a Dectris Mythen 1 K detector. For visualization and indexation, the software WinXPOW was used.[29]

SEM/EDS: Crystals for SEM/EDS measurements were prepared and selected in a glove box under inert gas atmosphere. Measurements were performed on a Zeiss EVO® MA15 (Carl Zeiss Microscopy Deutschland GmbH, Oberkochen) using the software SmartSEM® Version 6.05 with accelerating voltage of 20 kV. For EDS measurements a Bruker Quantax 200-Z3 Xflash630 (Bruker Corporation, Billerica, USA) was used as X-ray detector with the software Bruker Esprit 2.1.2.

Acknowledgments

The authors thank Prof. Korber and Prof. Pfitzner for providing laboratory space and equipment, Prof. Röhr, Bernard Lehmann for valuable discussions, Florian Wegner (AK Prof. Pfitzner) for powder diffraction experiments and Ferdinand Gigl and Marc Schlosser (AK Prof. Pfitzner) for SEM/EDS measurements and evaluation. This research was funded by the German Science Foundation (DFG) (GA 2504/1-1). Open Access funding enabled and organized by Projekt DEAL.

Conflict of Interest

The authors declare no conflict of interest.

Data Availability Statement

The data that support the findings of this study are available in the supplementary material of this article.

Keywords: Thallium · X-Ray structure · alkali metals · single crystals · large x-ray absorption coefficient

[1] E. Zintl, W. Dullenkopf, *Z. Phys. Chem.* **1932**, *B16*, 195–205.
[2] S. Gärtner, *Crystals* **2020**, *10*, 1013.
[3] R. Pöttgen, D. Johrendt, *Intermetallics*, 2nd ed., deGruyter, Berlin/Boston, **2019**, pp. 117–122.
[4] a) Z. C. Dong, J. D. Corbett, *J. Am. Chem. Soc.* **1993**, *115*, 11299–11303; b) Z. C. Dong, J. D. Corbett, *J. Am. Chem. Soc.* **1994**, *116*, 3429–3435; c) Z.-C. Dong, J. D. Corbett, *J. Cluster Sci.* **1995**, *6*, 187–201; d) Z. C. Dong, J. D. Corbett, *Inorg. Chem.* **1996**, *35*, 2301–2306; e) Z. C. Dong, J. D. Corbett, *Inorg. Chem.* **1996**, *35*, 3107–3112; f) B. Li, J. D. Corbett, *J. Cluster Sci.* **2008**, *19*, 331–340; g) S. Kaskel, J. D. Corbett, *Inorg. Chem.* **2000**, *39*, 778–782; h) S. Gärtner, S. Tiefenthaler, N. Korber, S. Stempfhuber, B. Hischa, *Crystals* **2018**, *8*.
[5] Z. C. Dong, J. D. Corbett, *J. Am. Chem. Soc.* **1995**, *117*, 6447–6455.
[6] *Chemistry, Structure and Bonding of Zintl Phases and Ions*, VCH Publishers, Inc., New York, Weinheim, Cambridge, **1996**.
[7] a) H. Schäfer, B. Eisenmann, W. Müller, *Angew. Chem. Int. Ed.* **1973**, *12*, 694–712; *Angew. Chem.* **1973**, *85*, 742–760; b) R. Nesper, *Z. Anorg. Allg. Chem.* **2014**, *640*, 2639–2648.
[8] F. Laves, *Naturwissenschaften* **1941**, *29*, 244–255.
[9] a) F. X. Pan, B. Weinert, S. Dehnen, in *50th Anniversary of Electron Counting Paradigms for Polyhedral Molecules: Bonding in Clusters, Intermetallics and Intermetalloids, Vol. 188* (Ed.: D. M. P. Mingos), Springer International Publishing Ag, Cham, **2021**, pp. 103-148; b) M. Falk, C. Meyer, C. Röhr, *Z. Anorg. Allg. Chem.* **2017**, *643*, 2070–2082; c) M. Falk, C. Röhr, *Z. Krist.-Cryst. Mater* **2019**, *234*, 623–646; d) M. Falk, M. Wendorff, C. Röhr, *Crystals* **2020**, *10*, 25; e) J. E. McGrady, F. Weigend, S. Dehnen, *Chem. Soc. Rev.* **2022**, *51*, 628–649.
[10] V. F. Schwinghammer, S. M. Tiefenthaler, S. Gärtner, *Materials* **2021**, *14*, 7512.
[11] Z. C. Dong, J. D. Corbett, *Inorg. Chem.* **1996**, *35*, 1444–1450.
[12] G. Cordier, V. Müller, *Z. Naturforsch. B* **1993**, *48*, 1035–1040.
[13] G. Cordier, V. Muller, *Z. Naturforsch. B* **1994**, *49*, 935–938.
[14] Z. C. Dong, J. D. Corbett, *Inorg. Chem.* **1995**, *34*, 5709–5710.
[15] Z. C. Dong, J. D. Corbett, *Angew. Chem. Int. Ed.* **1996**, *35*, 1006–1009; *Angew. Chem.* **1996**, *108*, 1073–1076.
[16] G. Cordier, V. Müller, R. Fröhlich, *Z. Kristallogr.* **1993**, *203*, 148–149.
[17] S. C. Sevov, J. D. Corbett, *Inorg. Chem.* **1993**, *32*, 1612–1615.
[18] 171.41.93a ed., Oxford Diffraction/Agilent Technologies UK Ltd, Yarnton, England, **2020**.
[19] U. Müller, in *Anorganische Strukturchemie, Vol. 6. aktualisierte Auflage*, Vieweg und Teubner, Wiesbaden, **2008**.
[20] S. Tiefenthaler, N. Korber, S. Gärtner, *Materials* **2019**, *12*; S. M. Tiefenthaler, M. Schlosser, F. Pielnhofer, I. G. Shenderovich, A. Pfitzner, S. Gärtner, *Z. Anorg. Allg. Chem.* **2020**, *646*, 82–87.
[21] B. Lehmann, C. Röhr, *Z. Kristallogr. Suppl.* **2022**, *42*, in press. (Annual Conference of the Crystallographic Society (DGK) 2022).
[22] K. Meindl, J. Henn, *Acta Crystallogr. Sect. A* **2008**, *64*, 404–418.
[23] F. Kleemiss, O. V. Dolomanov, M. Bodensteiner, N. Peyerimhoff, L. Midgley, L. J. Bourhis, A. Genoni, L. A. Malaspina, D. Jayatilaka, J. L. Spencer, F. White, B. Grundkotter-Stock, S. Steinhauer, D. Lentz, H. Puschmann, S. Grabowsky, *Chem. Sci.* **2021**, *12*, 1675–1692.
[24] O. V. Dolomanov, L. J. Bourhis, R. J. Gildea, J. A. K. Howard, H. Puschmann, *J. Appl. Cryst.* **2009**, *42*, 339–341.
[25] L. Hackspill, *Helv. Chim. Acta* **1928**, *11*, 1003–1026.
[26] G. M. Sheldrick, *Acta Crystallogr. Sect. A* **2015**, *71*, 3–8.
[27] G. M. Sheldrick, *Acta Crystallogr. Sect. C* **2015**, *71*, 3–8.
[28] K. Brandenburg, 4.6.6 ed., Crystal Impact GbR, Bonn, **2021**.
[29] 3.4.6 ed., STOE & Cie GmbH, Darmstadt, **2016**.

Manuscript received: March 25, 2022
Revised manuscript received: May 16, 2022
Accepted manuscript online: May 27, 2022

